Theoretical modeling and finite element analysis of the contact width of O-ring rubber seals

Liu Peng, Yin Chuan, Huang Long, Zhang Peng, Lin Lijun

(College of Mechanical Engineering, Chengdu University, Chengdu 610106, Sichuan, China)

Abstract: As a crucial downhole flow control tool, the O-ring contact width of the downhole intelligent sliding sleeve is a key parameter for assessing the sealing performance of the tool. This paper establishes a contact width prediction model for the O-ring seal in petroleum downhole applications. Based on the Hertz contact theory, the Mooney-Rivlin hyperelastic theory is introduced to characterize the nonlinear mechanical properties of rubber materials, and the expression for contact width is derived. The ANSYS finite element analysis results show that the average error of the established contact width prediction model is 5.9%, with a minimum error of only 1.6% and a maximum error of 10.9%. This provides theoretical support and data reference for the structural design, performance optimization, and engineering application of O-ring rubber seals in petroleum downhole applications.

Key words: smart sliding sleeve; O-ring; contact width; super-elasticity; finite element simulation

Classification number: TQ336.42 **Article number:** 1009-797X(2026)02-0056-07

Document code: B **DOI:**10.13520/j.cnki.rpte.2026.02.014

As the core tool for regulating underground fluid movement, the sealing reliability of the intelligent sliding sleeve directly determines the safety of the entire equipment. In the sealing structure of the sliding sleeve, the sealing ring plays a crucial role in blocking leakage and maintaining pressure difference. The O-ring rubber seal, with its advantages of simple structure, convenient assembly and disassembly, and reliable sealing performance, possesses excellent sealing adaptability and assembly/disassembly convenience. It is an important foundation for ensuring the long-term stable and reliable operation of the sliding sleeve under high pressure difference conditions. The contact width of the O-ring directly affects the sealing performance and service life. If the contact width is too large, it will lead to a sharp increase in friction, accelerating the wear of the sealing ring; if the contact width is insufficient, it will be difficult to establish effective sealing, which can easily lead to underground leakage or even safety accidents.

Currently, Zheng Wenming et al. have elaborated on the design criteria for the contact width of O-rings based on their long-term experience and understanding in hydraulic and lubrication equipment management. Rao Jianhua conducted a finite element analysis on the stress and contact pressure of O-shaped rubber seals and retaining rings under different pressures, analyzing the relationship between the contact pressure and contact width of O-shaped rubber seals. Xia Zhi et al. explored the sealing performance of O-rings under different compression rates based on fluid-structure coupling simulation analysis. Liu Peng et al. studied the sealing performance of O-rings under different hardnesses and working conditions, discussing the influence of material hardness, radial compression rate, and external pressure on the sealing contact pressure of O-rings. Wang Zhixiang et al. utilized the automatic shrink fit method in finite element software to simulate the radial assembly process of composite seals, analyzing the impact of different parameters on rubber seals.

Biography: Liu Peng (2001-), male, is a graduate student majoring in Mechanical Engineering, with his main research interests lying in the development and application of downhole intelligent tools and intelligent instruments.

Artur Karaszkiewicz et al. derived the relationship between the contact width of O-rings, compression rate, and cross-sectional diameter through experimental methods and simulation analysis.

Upon reviewing existing research findings, it is evident that the current mainstream O-ring contact width formulas primarily consider only two geometric parameters: the compression ratio and the cross-sectional diameter of the O-ring, without taking into account the inherent properties of the sealing ring material, such as hardness. This limitation restricts the applicability and prediction accuracy of the formulas. To address this shortcoming, this paper, framed by Hertz's contact theory, introduces the Mooney-Rivlin hyperelastic theory. It incorporates the hardness parameter HA, which characterizes the mechanical properties of rubber materials, as well as hyperelastic constitutive parameters (such as C_{10} and C_{01}), into the modeling scope. Consequently, a new prediction model for the contact width of O-ring rubber seals is reconstructed, and its correctness is verified through finite element analysis.

1 Theoretical model

After compression, the O-ring makes line contact with the sealing surface. The contact width can be analyzed based on Hertz's contact theory, which was established to address contact problems of linearly elastic bodies. When dealing with contact problems of hyperelastic materials such as rubber, it is necessary to correct the radius of curvature and equivalent elastic modulus of the compressed O-ring. The contact width of the O-ring is:

$$w=2\sqrt{\frac{FR^*}{\pi E^*}} \tag{1}$$

In the formula: w represents the contact width of the O-ring, in millimeters; F denotes the normal force, in newtons; R^* signifies the radius of curvature, in millimeters; and E^* stands for the equivalent elastic modulus, in megapascals.

1.1 Normal force

Rubber is a super-elastic material. Due to its closer proximity to the actual behavior of rubber materials, the Mooney-Rivlin model is the most widely used. Therefore, the constitutive model for O-ring materials adopts the Mooney-Rivlin model, commonly using a 2-parameter model. The strain energy density function W is:

$$W=C_{10}(I_1-3)+C_{01}(I_2-3) \tag{2}$$

In the formula, I_1 represents the first Green strain invariant, and I_2 represents the second Green strain invariant. The relationship is as follows:

$$I_1=\lambda^2_1+\lambda^2_2+\lambda^2_3 \tag{3}$$

$$I_2=\lambda^2_1\lambda^2_2+\lambda^2_2\lambda^2_3+\lambda^2_3\lambda^2_1 \tag{4}$$

In the formula, λ_1, λ_2, $\lambda_3$represent the elongation ratio or compression ratio in the directions of main axes 1, 2, and 3, respectively.

The deformation gradient tensor $F=\mathrm{diag}(\lambda_1,\lambda_2,\lambda_3)=\mathrm{dian}((1-\varepsilon)^{-\frac{1}{2}},(1-\varepsilon)^{-\frac{1}{2}},(1-\varepsilon)$(ε representing the axial compressibility) satisfies, $\varepsilon F=\lambda_1\lambda_2\lambda_3=1,\lambda_1=\lambda_2=(1-\varepsilon)^{-\frac{1}{2}},\lambda_3=1-\varepsilon$,and . For the left Cauchy-Green deformation tensor$B=FF^{\mathrm{T}}=\mathrm{dian}(\lambda^2_1,\ \lambda^2_2,\ \lambda^3_3)$, the relationship between I_1 and I_2 is as follows:

$$I_1=\mathrm{tr}(B)=\lambda^2_1+\lambda^2_2+\lambda^2_3=2(1-\varepsilon)^{-1}+(1-\varepsilon)^2 \tag{5}$$

$$I_1=\frac{1}{2}[(\mathrm{tr}B)^2-\mathrm{tr}(B^2)=\lambda^2_1\lambda^2_2+\lambda^2_2\lambda^2_3+\lambda^2_3\lambda^2_1=(1-\varepsilon)^{-2}+2(1-\varepsilon) \tag{6}$$

For rubber materials, the nominal stress (Piola-Kirchhoff stress) P can be obtained by taking the partial derivative of the strain energy function W with respect to the deformation gradient. Therefore, the nominal stress P is:

$$P=\frac{\partial W}{\partial\lambda_1}=\frac{\partial W}{\partial I_1}\frac{\partial I_1}{\partial\lambda_1}+\frac{\partial W}{\partial I_2}\frac{\partial I_2}{\partial\lambda_1}=2(C_{10}+C_{01})\varepsilon+3(C_{10}+3C_{01})\varepsilon^2 \tag{7}$$

The nominal stress P acts on the reference area, and the actual normal force F is:

$$F=\pi R^2[2(C_{10}+C_{01})\varepsilon+3(C_{10}+3C_{01})\varepsilon^2] \tag{8}$$

1.2 radius of curvature

(1) Initial geometric state (uncompressed)

When the O-ring is not compressed, its cross-section is a standard circle, and the radius of curvature of the circular cross-section is equal, both being $\frac{d}{2}$(d represents the cross-sectional diameter).

(2) Geometric deformation after compression (post-compression)

When the O-ring is subjected to axial compression, due to the incompressibility of rubber material (volume conservation), the cross-sectional shape changes from circular to approximately elliptical, with the cross-sectional

area remaining equal before and after compression. After compression, the short axis of the ellipse is b and the long axis is a. Therefore, the short axis of the ellipse, $b=R(1-\varepsilon)$the initial circular cross-sectional area, and the compressed elliptical cross-sectional area are πR^2 , and respectively. According to the conservation of area πab. the long axis a of the ellipse is:

$$\pi ab=\pi R^2 \Rightarrow a=\frac{R}{1-\varepsilon} \tag{9}$$

(3) Radius of curvature

For the compressed elliptical cross-section, contact occurs at the vertex of the ellipse (the maximum deformation point under axial compression), with a radius of curvature being:

$$R'=\frac{a^2}{b}=\frac{\left(\frac{R}{1-\varepsilon}\right)^2}{R(1-\varepsilon)}=\frac{R}{(1-\varepsilon)^3} \tag{10}$$

1.3 Equivalent elastic modulus

The elastic modulus E, C10, and C01 coefficients of rubber can be determined based on the hardness HA of rubber according to the following formula:

$$E=\frac{15.75+2.15H_A}{100-H_A} \tag{11}$$

$$C_{01}=0.25C_{10} \tag{12}$$

$$E=6(C_{10}+C_{01}) \tag{13}$$

In the formula, C_{10} and C_{01} represent the Mooney-Rivlin parameters.

The elastic modulus of rubber materials exhibits significant strain nonlinearity under large deformation, necessitating the introduction of correction terms to enhance model accuracy. Through static tensile tests on nitrile rubber, a fitting was obtainedC_{10}=0.115 9 MPa,C_{01}=0.0.214 7 MPa, validating the rationality of the basic elastic modulus $E=6(C_{10}+C_{01})$ and indicating that additional correction is required to control the error within 5% under large strain. Research on O-rings for shield machines shows that when the compression rate is between 10% and 25%, the contact stress is linearly correlated with strain. The linear correction form can control the prediction error within 7%, supporting 1+2.5ε the engineering applicability of the correction term. The extended Mooney-Rivlin model further verifies the universality of the strain correction term, and its results are highly consistent with experimental data on rubber. In summary, the strain correction term adopted in this paper has both experimental and theoretical support, and is well compatible with the mechanical laws of rubber materials. Therefore, the equivalent elastic modulus E^* is:

$$E^*=6(C_{10}+C_{01})\ (1+2.5\varepsilon) \tag{14}$$

Based on equations (1) to (14), the contact width of the O-ring is:

$$w=2\sqrt{\frac{FR'}{\pi E^*}}=\sqrt{\frac{d^2\left[2(C_{10}+C_{01})\varepsilon+3(C_{10}+3C_{01})\varepsilon^2\right]}{12(1-\varepsilon)^3(C_{10}+C_{01})(1+2.5\varepsilon)}} \tag{15}$$

2 Geometric simulation model

Taking a certain intelligent sliding sleeve as an example, the O-ring is placed in the sealing groove of the part, and the sealing type is static sealing. The sealing is achieved by the deformation of the O-ring under pressure, as shown in figure 1. The O-ring is prone to damage during assembly, and its compression rate is only affected by the space reserved in the structure. This article analyzes the sealing performance of the O-ring and studies the contact width and mechanical properties of the O-ring under different compression rates.

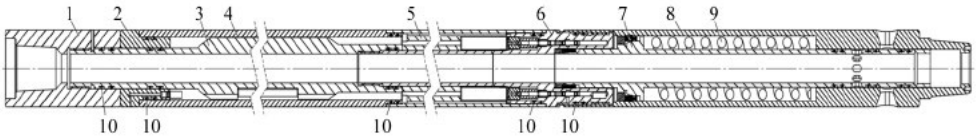

1-Outer joint, 2-Upper joint, 3-Spindle, 4-Outer cylinder, 5-Storage chamber sub, 6-Motion sub, 7-Inner sliding sleeve, 8-Outer sliding sleeve, 9-Circular cross-section helical compression spring, 10-O-shaped rubber sealing ring

Figure 1 2D model of smart slide cover

Given that both the O-ring and the sealing groove exhibit axisymmetric characteristics, to simplify calculations and enhance efficiency, the three-dimensional solid model is simplified to a two-dimensional axisymmetric model, as illustrated in figure 2.

The finite element simulation analysis of the O-ring was conducted using ANSYS software. The O-ring selected for the simulation was a 2-331 standard part produced by Parker, with an inner diameter of 56.52 mm and a diameter of 5.33 mm. Considering the characteristics of the petroleum downhole

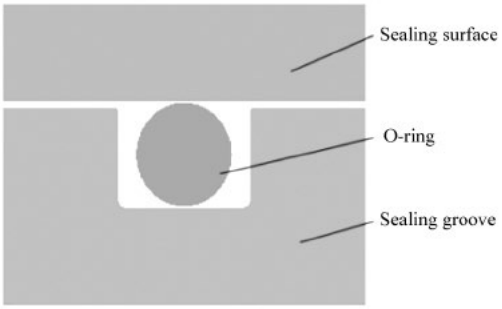

Figure 2 Simplified model of O-ring sealing area

environment, such as high temperature and strong corrosivity, the sealing ring material was selected as nitrile rubber, with a Poisson's ratio v=0.499. The Shore hardness range of this material is typically 20-90. In this study, four grades of Shore hardness, namely 60, 70, 80, and 90, were selected, and corresponding material parameters were obtained accordingly. Details are shown in table 1. Both the sealing groove and sealing surface materials were structural steel, with an elastic modulus of 2×10^5 MPa and a Poisson's ratio v=0.3.

Table 1 Parameters of nitrile rubber materials with different hardnesses

Hardness (H_A)	60	70	80	90
E(MPa)	3.619	5.542	9.388	20.925
C_{10}(MPa)	0.483	0.739	1.252	2.790
C_{01}(MPa)	0.121	0.185	0.313	0.698

When analyzing using this two-dimensional axisymmetric model, the following assumptions are made:

(1) Isotropic, continuous and uniform;

(2) The displacement and deformation of the O-ring are centrosymmetric;

(3) Ignoring the impact of medium temperature changes on the O-ring material, the medium temperature remains constant during the analysis process.

Based on the aforementioned parameters, a corresponding solid model was established in ANSYS software, with the dimensions of the sealing groove designed according to Parker standards. To enhance the mesh quality, all areas were discretized using quadrilateral elements. Considering that the O-ring is a super-elastic material with an elastic modulus much lower than that of structural steel, the mesh was refined in the O-ring area, especially with local densification in the contact area, to improve computational convergence and solution accuracy. To reasonably control the computational scale, the mesh size in the sealing surface and sealing groove areas was appropriately relaxed to 0.5 mm. However, the mesh size in the O-ring area was set to 0.2 mm, with local densification implemented, as shown in figure 3.

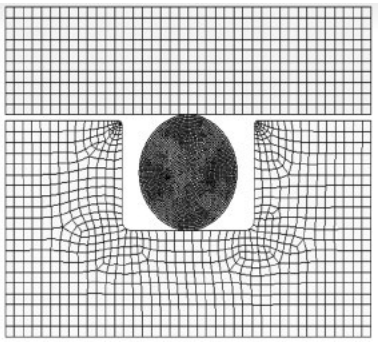

Figure 3 Partial grid diagram of O-ring sealing area

To simulate the pre-compression process of the O-ring, the sealing groove is set as a fixed support boundary condition, and a displacement load is applied on the sealing surface to make it close perfectly with the sealing groove. To further analyze the contact behavior of the sealing ring during the compression process, contact pairs are established between the O-ring and the sealing groove, as well as between the O-ring and the sealing surface. In the contact pair formed by the O-ring and the sealing groove, the surface of the O-ring is defined as the contact surface, and the surface of the sealing groove is defined as the target surface, as shown in figure 4(a). Correspondingly, in the contact pair formed by the O-ring and the sealing surface, the surface of the O-ring is the contact surface, and the sealing surface is the target surface, as shown in figure 4(b). All contact types are set as frictional contact, with a friction coefficient of 0.3, and the generalized Lagrange algorithm is used for solving.

3 Result analysis

In this study, an O-ring with HA=90 was selected as the simulation object, and its mechanical states under eight different compression rates, namely 7.5%, 10%, 12.5%, 15%, 17.5%, 20%, 22.5%, and 25%, were deeply investigated. The obtained compression deformation patterns are shown in figure 5. It can be clearly observed from Figure 5 that as the compression rate gradually increases, the deformation degree of the O-ring shows a significant increasing trend. At lower compression rates (such as 7.5%-15%), the deformation of the

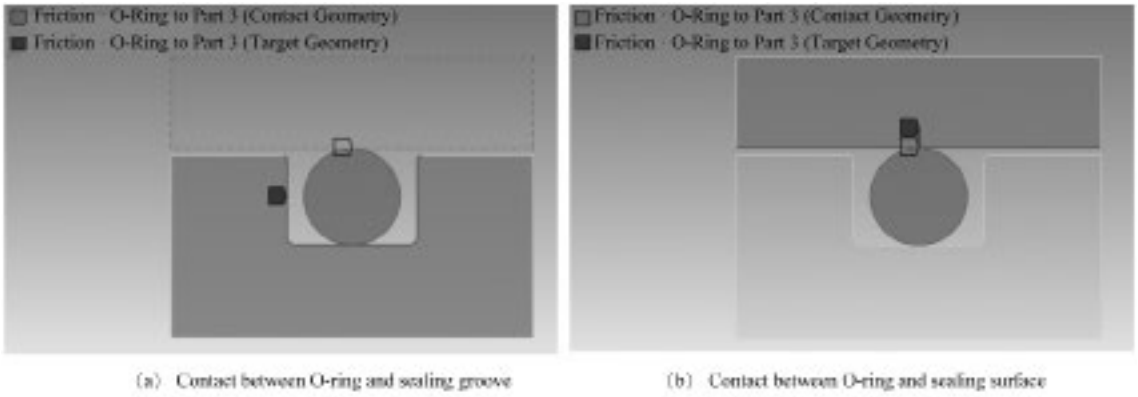

(a) Contact between O-ring and sealing groove (b) Contact between O-ring and sealing surface

Figure 4 Contact pair diagram of O-ring sealing area

O-ring is relatively smooth, and although the overall shape changes, it still maintains a good approximation to a circular contour feature. However, when the compression rate further increases (such as 17.5%-25%), the deformation of the O-ring becomes more pronounced, the squeezing effect with the contact interface intensifies, and the shape gradually evolves towards an elliptical shape. The deformation differences under different compression rates are also more visually prominent, which intuitively reflects that the compression rate has a significant impact on the mechanical response and deformation behavior of the O-ring.

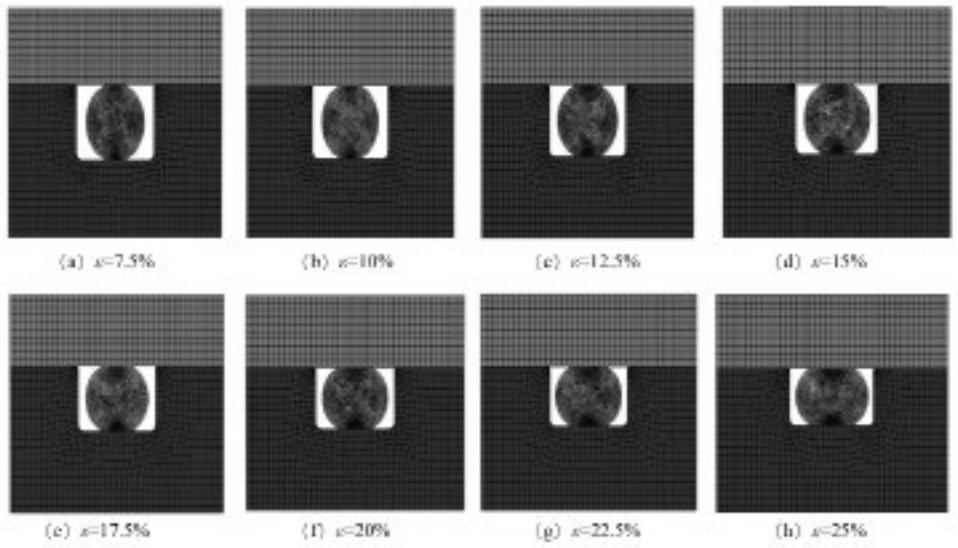

(a) ε=7.5% (b) ε=10% (c) ε=12.5% (d) ε=15%

(e) ε=17.5% (f) ε=20% (g) ε=22.5% (h) ε=25%

Figure 5 Compression state of O-rings with different compression rates

Using different compression rates as variables, calculations and simulations were conducted on O-rings with a hardness of 90. The average error between the theoretical calculation results and the simulation analysis results for contact width was 5.9%, with a minimum error of 1.6% and a maximum error of 10.9%, as shown in table 2.

Table 2 Table of contact width for O-rings with HA=90

compression ratio	7.50%	10%	12.50%	15%	17.50%	20%	22.50%	25%
Simulation analysis / mm	1.503	1.801	2.024	2.336	2.551	2.769	3.102	3.337
Theoretical calculation / mm	1.527	1.831	2.128	2.428	2.735	3.055	3.39	3.746
error	1.6	1.6	4.9	3.8	6.7	9.4	8.5	10.9

To further investigate the impact of hardness on the contact width of O-rings, O-rings with hardnesses of 60, 70, and 80 were selected for calculation and simulation. The results showed consistency between the calculated and simulated

outcomes for different hardnesses. Referring to the curves in figure 6(a)-(d) depicting the variation of contact width of O-rings with different hardnesses as a function of compression ratio, it is evident that under conditions of minor differences in Shore hardness, the contact widths of the O-rings remain essentially consistent. Furthermore, the contact widths exhibit an approximately linear increase with increasing compression ratio, indicating that the compression ratio is a key factor affecting the contact width of O-rings. However, within a narrow range of hardness variation, the impact of hardness on the contact width is not significant.

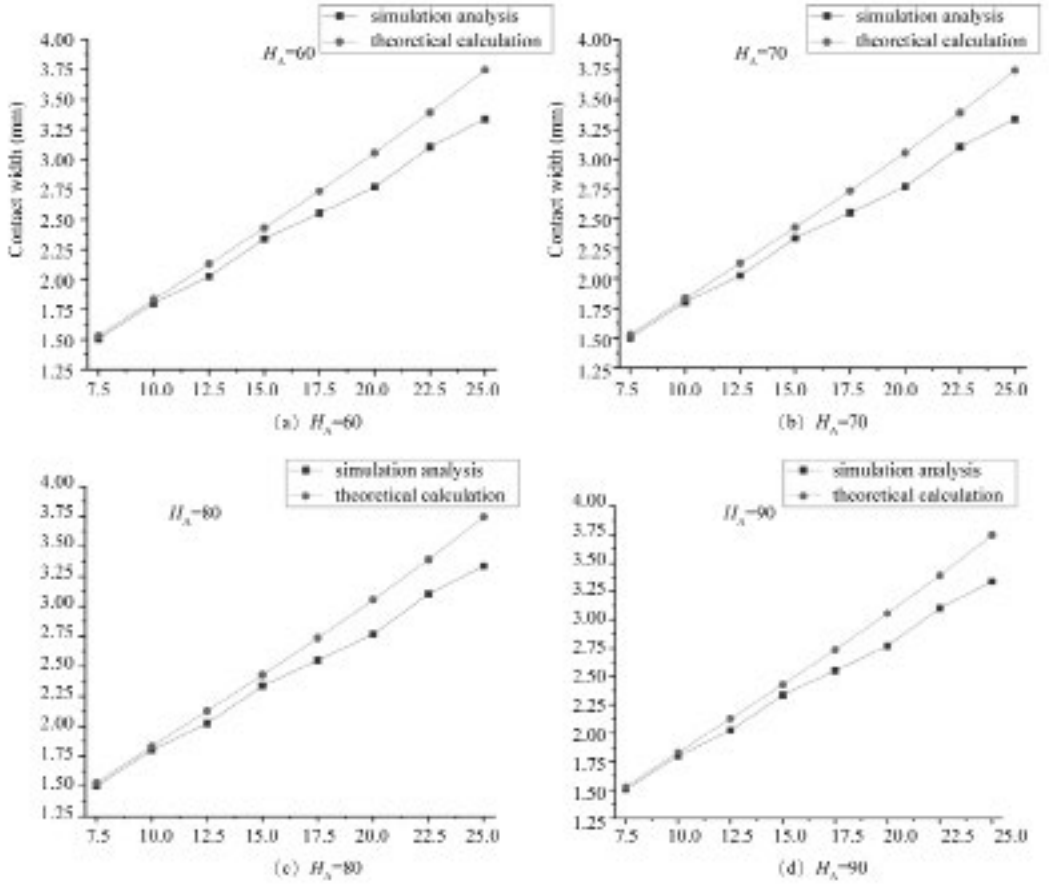

Figure 6 Diagram of contact width of O-rings with different hardnesses

During the compression process of the O-ring, both the contact pressure and the equivalent pressure exhibit an increasing trend as the compression ratio increases. From the pressure variation curves under different hardnesses (HA=60, 70, 80, 90) shown in figures 7 and 8, it is clear that the greater the material hardness, the higher the overall level of pressure. When HA=90, the values of contact pressure and equivalent pressure are significantly higher than those when HA=60. Additionally, there is some fluctuation in the early stage of pressure, but in the later stages of compression, both contact pressure and equivalent pressure tend to rise steadily, exhibiting a relatively consistent pattern of change.

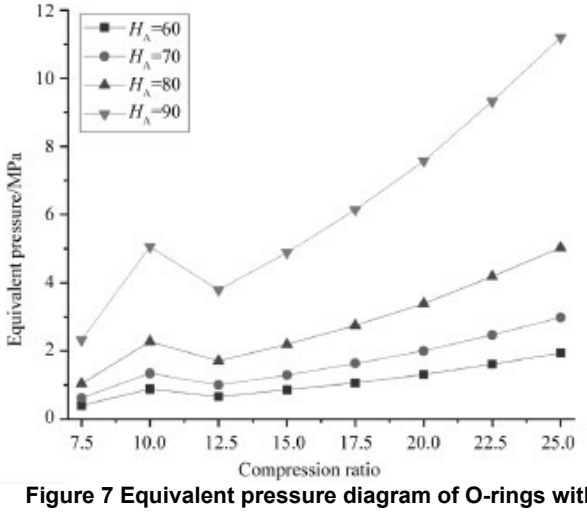

Figure 7 Equivalent pressure diagram of O-rings with different hardnesses

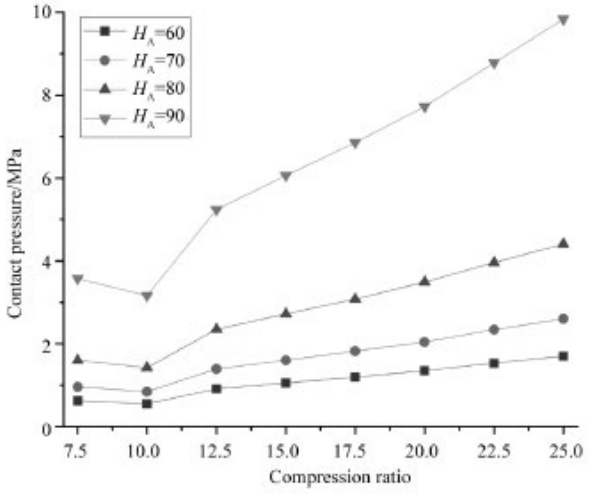

Figure 8 Contact pressure diagram of O-rings with different hardnesses

4 Conclusion

This study takes the O-ring used in a certain intelligent sliding sleeve as the research object and draws the following conclusions:

(1) By revising the Hertz contact theory and incorporating the Mooney-Rivlin hyperelastic constitutive model, a theoretical prediction model suitable for the contact width of O-rings was established. Within the compression ratio range of 7.5% to 25%, multiple working conditions were selected for verification. The results indicated that the average error of the theoretical model was 5.9%, with a minimum error of 1.6% and a maximum error of 10.9%.

(2) The contact width of the O-ring rubber seal increases significantly with the increase in compression ratio; in cases where there is little difference in Shore hardness, the contact widths of O-rings with different hardnesses tend to be consistent. This indicates that the compression ratio is a key factor affecting the contact width of the O-ring, while the impact of hardness on the contact width is not significant when there is only a small range of hardness variation.

(3) When the O-ring is compressed, an increase in compression ratio leads to an increase in both contact pressure and equivalent pressure; the greater the material hardness, the higher the overall pressure level; the pressure fluctuates in the early stage and tends to rise steadily in the later stage, with the variation patterns gradually becoming consistent.